Crucial role of interlayer distance for antiferromagnet-induced perpendicular magnetic anisotropy

Bo-Yao Wang,[1,*] Po-Han Lin,[1] Ming-Shian Tsai,[1] Chun-Wei Shih,[1] Meng-Ju Lee,[1] Chun-Wei Huang,[1] Nae-Yeou Jih,[2] Pei-Yu Cheng,[3] and Der-Hsin Wei[3]

[1]*Department of Physics, National Changhua University of Education, Changhua 500, Taiwan*

[2]*The Center of Teacher Education, National Chung Hsing University, Taichung 402, Taiwan*

[3]*National Synchrotron Radiation Research Center, Hsinchu 300, Taiwan*

(Received 1 October 2015; revised manuscript received 3 November 2015; published 28 December 2015; corrected 25 May 2016)

Antiferromagnetic (AFM) thin films were recently proposed to be an alternative to conventional materials for achieving perpendicular magnetic anisotropy (PMA) in ferromagnetic thin films, because AFM thin films exhibit an advantage of flexible control. Here, we report that antiferromagnet-induced PMA is highly sensitive to interfacial moments of AFM thin films as well as the magnetic interaction of such moments with volume moments, determined according to the vertical interlayer distance. Magnetic hysteresis loops and x-ray magnetic domain imaging revealed the establishment of perpendicular magnetization on face-centered tetragonal (fct)-like Mn/Co/Ni films when covered with monolayered Mn films. A cover of Mn films that exhibit contracted fct-[vertical-to-in-plane lattice constant ratio (c/a) = 0.95] and expanded fct-like (c/a = 1.05) structures at different thickness levels induced in-plane magnetic anisotropy and PMA in Co/Ni films, respectively, confirming that the interlayer distance is a crucial parameter for establishing perpendicular magnetization.

DOI: 10.1103/PhysRevB.92.214435 PACS number(s): 75.70.Kw, 75.30.Gw, 75.50.Ee

I. INTRODUCTION

Antiferromagnets have attracted considerable research interest in the field of magnetism because of their effective applicability to current magnetological devices, such as spin valves [1,2], and rich physics that can be explored. According to research efforts in recent years, antiferromagnetic (AFM) layers can exert various effects such as coercivity (H_c) enhancement, exchange bias field, and magnetization switching on adjacent ferromagnetic (FM) layers [3–13]. Although coercivity enhancement and exchange bias field have been extensively investigated in the past two decades, magnetization switching was discovered only in recent years. Several studies have suggested that magnetization reorientation can be induced by a magnetic frustration at the AFM/FM interface [8–10]. Other studies have revealed that the induced magnetic anisotropy is strongly correlated with the uncompensated moments of the AFM layer at the FM/AFM interface [11,12]. According to the observations of these studies, AFM films can induce perpendicular magnetic anisotropy (PMA) on adjacent FM layers [11–13]. Vital PMA parameters can be flexibly manipulated by tuning the thicknesses in AFM/FM bilayers [14,15], thus providing an additional degree of freedom for controlling the perpendicular magnetization desired in current magnetic devices [16–19]. Nevertheless, because the key parameters of AFM films inducing PMA are still unclear, the phenomenon of antiferromagnet-induced PMA is currently demonstrated only in limited systems such as face-centered-cubic (fcc)-Mn/FM [11,12] and CoO/Ni [13] bilayer films. Generalizing this phenomenon into real applications necessitates additional research efforts. A study on fcc-Mn/FM bilayers reported that antiferromagnet-induced PMA is associated with the interfacial uncompensated moments of an Mn layer demonstrating an established perpendicular crystalline anisotropy [12]. Moreover, the Mn layer thickness governs the thermal stability of PMA, which is described according to the finite-size effects of low-dimensional antiferromagnets [11,20]. These findings suggest that antiferromagnet-induced PMA is associated with the magnetic interaction between interfacial moments and other moments within the volume of the Mn film, indicating that the crystalline structure of the Mn film may be a crucial factor responsible for the antiferromagnet-induced PMA phenomenon. To further clarify this critical phenomenon, we investigated a face-centered tetragonal (fct)-like Mn/FM film; the crystalline structure of this Mn film slightly deviates from that of a previously reported fcc-Mn film [11]. According to previous reports [21,22], fct-like Mn films can be grown epitaxially on Co/Cu(001). The magnetic anisotropy of the FM layer can be controlled to be either in-plane or out-of-plane by incorporating the Ni film as an underlayer of the Co film and tuning the relative thicknesses [23]. This enables designing a system model of fct-like Mn/Co/Ni/Cu(001) films that induce weak in-plane magnetic anisotropy (IMA) in adjacent FM films; such a model is suitable for probing the phenomenon of Mn-film-induced magnetic anisotropy and clarifying the structural effects of antiferromagnets on PMA.

In this study, we investigated the structural effects of ultrathin AFM films on the corresponding PMA they induce by comparing the crystalline structure and magnetic behaviors of epitaxially grown fct-like Mn/Co/Ni/Cu(001) films. We observed a substantial modulation on the effect of the induced PMA, which occurred concurrently as the interlayer distance of the Mn films was changed and the thickness of the Mn films was varied. The findings provide clear experimental evidence that the interlayer distance of AFM films, which regulate the magnetic interaction between interfacial moments and moments within the volume, is a crucial parameter responsible for the induced PMA in AFM/FM films.

II. EXPERIMENT

Samples of Mn/Ni/Co films were prepared and investigated *in situ* in an ultrahigh vacuum preparation chamber with

*bywang1735@cc.ncue.edu.tw

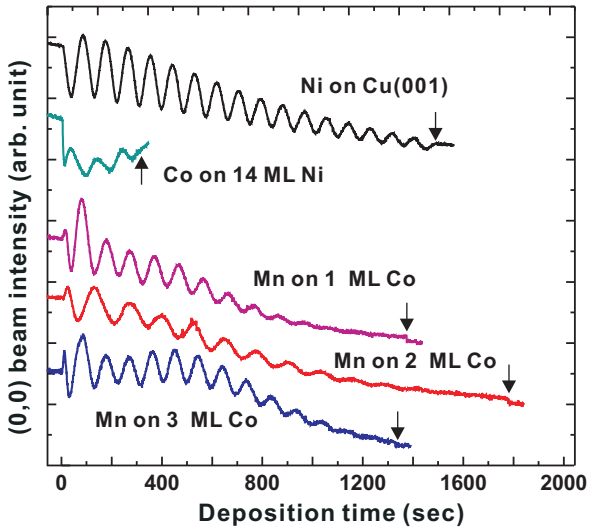

FIG. 1. (Color online) Selected MEED (0,0) beam intensity curves as functions of deposition time for the Ni film grown on Cu(001), Co film grown on 14 ML Ni/Cu(001), and Mn film grown on 1–3 ML Co/14 ML Ni/Cu(001) at 300 K. The thickness of films was calibrated by the oscillation in MEED curves. The arrows indicate the time for the close of the shutter.

a base pressure of 2×10^{-10} Torr. Cu(001) single-crystal substrates with a 0.1° miscut were cleaned by applying cycles of 2 keV Ar^+ ion sputtering and annealed at 800 K for 5 min to obtain a smooth morphology and an adequately ordered crystalline structure [24]. The growth rates were monitored using medium-energy electron diffraction (MEED). Figure 1 shows the specular MEED (0,0) beam intensity of the Ni film grown on Cu(001), the Co film grown on 14 ML Ni/Cu(001), and the Mn film grown on 1–3 ML Co/14 ML Ni/Cu(001). In each case, a presence of regular oscillation of the (0,0) beam intensity indicates a layer-by-layer growth mode of the films. When a 14 ML Ni film was deposited on Cu(001), the sample was annealed at 430 K for 10 min to improve the surface smoothness [25]. Either uniform or wedge-shaped Mn/Ni/Co films were deposited on the substrates for measuring the crystalline structure/magnetic hysteresis loop and magnetic domain imaging of the samples.

The average in-plane and interlayer distances of the films were determined using low-energy electron diffraction (LEED) with a kinematics approximation (LEED I/V) [26]. Magnetic hysteresis loops of the thin films were measured on the basis of the magneto-optical Kerr effect (MOKE) in both longitudinal and polar geometries. The magnetic domain images of Mn/Co bilayers were obtained *in situ* through photoemission electron microscopy (PEEM) [27,28] by observing x-ray magnetic circular dichroism (XMCD) effects at beam line BL05B2 of the national synchrotron radiation research center (NSRRC) in Hsinchu, Taiwan. The angle of incident right circularly polarized (RCP) x rays was 25° with respect to the in-plane $[0\bar{1}0]$ crystallographic direction of Cu(001). The magnetic information of individual elements can be derived according to the asymmetry of the XMCD curves at $L_{3,2}$ absorption edges [5]. The full-field view of the magnetic domain image was resolved by recording the secondary electrons emitted from the magnetic sample in PEEM. Contrast normalization was achieved by performing imaging calculations for the two full-field images taken at the Ni, Co, or Mn L_3 and L_2 edges by applying the formula $(I_{L3} - I_{L2})/(I_{L3} + I_{L2})$ [5], where I_{L3} and I_{L2} are the x-ray absorption intensity of the sample taken at the L_3 and L_2 edges, respectively. In the current study, magnetic imaging was performed under the as-grown condition at either 300 or 105 K.

III. RESULTS

A. Crystalline structure of Mn/Co/Ni/Cu(001) films

This section presents the crystalline structure of the Mn/Co/Ni films grown on Cu(001). Figures 2(a)–2(h) illustrate selected LEED patterns of Cu(001), subsequently deposited 2 ML Co/14 ML Ni films, and 1–14 ML Mn films grown on Co/Ni bilayers at 110 eV, respectively. The LEED P(1 × 1) spots of these films were clearly located at the same positions as that of Cu(001), indicating an epitaxial growth condition; this is consistent with the findings of a previous study [26]. Therefore, the in-plane lattice constant ($d_{\parallel}$) of the Mn and Co films was obtained from the Cu(001) value (approximately 3.61 Å). Figures 3(a) and 3(b) show selected LEED specular spot I/V curves and vertical interlayer distance ($d_{\perp}$) for the 1–3 ML Co/14 ML Ni films grown on Cu(001) and Mn films grown on the Co/Ni bilayers, respectively. The $d_{\perp}$ value of the 1–3 ML Co/14 ML Ni films is approximately 1.71 Å, which is similar to the value of Ni films grown on Cu(001) [29,30]. In addition, for Mn films grown on the Co/Ni bilayers, the $d_{\perp}$ value of thin Mn films (thickness of Mn films $t_{Mn} < 6$ ML) is 1.71 Å. However, in Fig. 3(a), there are two series of energy peaks (I) shown in the LEED I/V curve of 6 ML Mn/Co/14 ML Ni film. This suggests two coexisted $d_{\perp}$ values (1.71 Å and 1.88 Å) for $t_{Mn} = 6$ ML. Then, the $d_{\perp}$ value of the Mn films changed to approximately 1.88 Å when t_{Mn} is greater than 6 ML. The $d_{\perp}$ value of either the thin Mn films ($t_{Mn} < 6$ ML) or thick Mn films ($t_{Mn} > 6$ ML) was constant when the temperature dropped from 300 to 150 K. Notably, for the Mn films grown on Co/Cu(001), the phase with $d_{\perp} = 1.71$ Å was also observed when the t_{Mn} value was less than 3 ML [22,31]. The crystalline structure of the Mn films can be conventionally classified on the basis of the ratio of the vertical and in-plane lattice constants (i.e., the c/a ratio). In the present study, Mn film c/a ratios close to either 0.95 or 1.05 indicate the presence of c-fct or e-fct structures. The presence of two metastable fcc-like phases on Mn films is consistent with the findings of previous experimental studies [32,33] and theoretical calculation [34]. Moreover, Co films grown on the 14 ML Ni film revealed c-fct structures with a c/a value of approximately 0.95 (Figs. 2 and 3).

B. Magnetic properties and induced SRT in the fct-like Mn/Co/Ni/Cu(001) films

We first applied MOKE to investigate the magnetic properties of the fct-like Mn films grown on the Co/Ni bilayers. Figure 4(a) shows the magnetic hysteresis loops of the 0–3 ML Co/14 ML Ni films measured along the in-plane [100] and out-of-plane [001] directions at 300 K. The

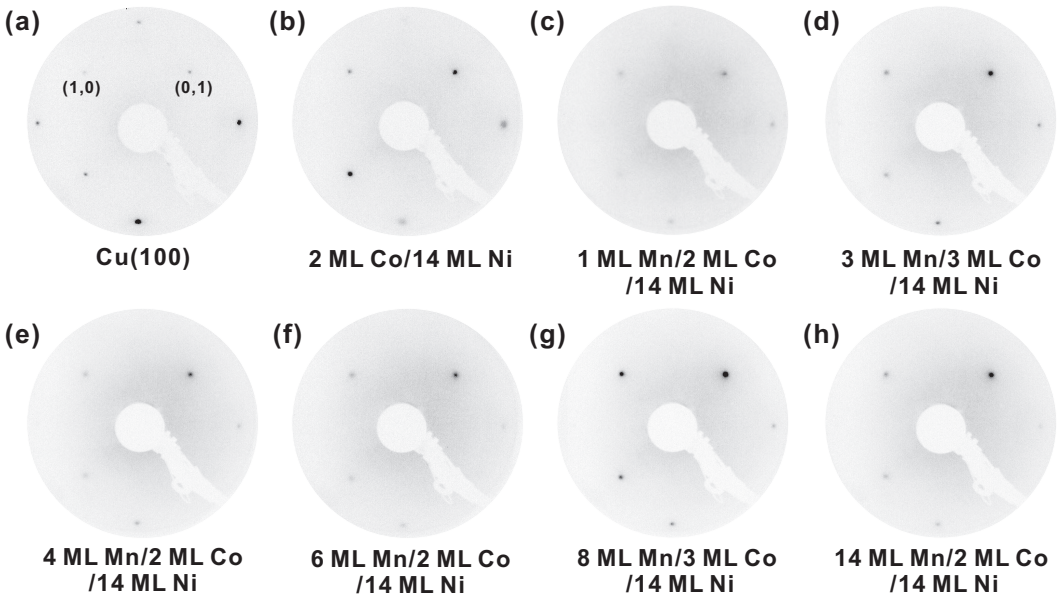

FIG. 2. LEED patterns of the (a) Cu(001), (b) 2 ML Co/14 ML Ni/Cu(001), (c) 1 ML Mn/2 ML Co/14 ML Ni/Cu(001), (d) 3 ML Mn/2 ML Co/14 ML Ni/Cu(001), (e) 4 ML Mn/2 ML Co/14 ML Ni/Cu(001), (f) 6 ML Mn/2 ML Co/14 ML Ni/Cu(001), (g) 8 ML Mn/2 ML Co/14 ML Ni/Cu(001), and (h) 14 ML Mn/2 ML Co/14 ML Ni/Cu(001) films, measured at 110 eV and 300 K.

14 ML Ni film demonstrated a characteristic PMA, which is contributed by a perpendicular magnetocrystalline anisotropy from the Ni films containing a c-fct structure [35]. When the Ni layer was further covered with the Co film, the magnetic anisotropy of the FM film changed from a perpendicular to an in-plane direction. This spin-reorientation transition (SRT) was induced by an enhanced IMA contributed by the shape anisotropy as well as the magnetocrystalline anisotropy of the Co film [35]. Figure 4(c) illustrates a magnetic easy axis phase diagram showing a summary of the magnetic anisotropy of the Co/Ni films covered with a Mn overlayer. For the 14 ML Ni film or Mn/Ni bilayers, the magnetic anisotropy was observed

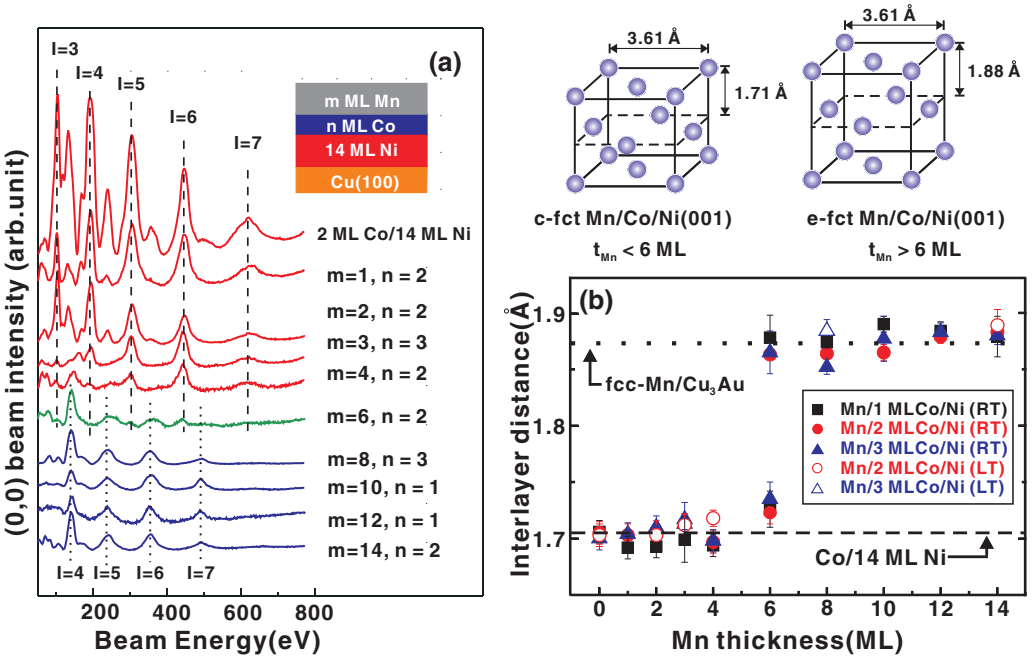

FIG. 3. (Color online) (a) Selected LEED specular spot I/V curves for various Mn films grown on the 1–3 ML Co/14 ML Ni/Cu(001) films measured at 300 K (RT). (b) Average interlayer distance ($d_\perp$) of various films calculated according to the energy peaks (I) in the I/V curves at RT or 150 K (LT). The $d_\perp$ of the Mn films changed from approximately 1.71 to 1.88 Å when $t_{Mn} > 6$ ML. In (b), the dashed line at the bottom represents $d_\perp$ of the 1–3 ML Co films grown on Cu(001); the dotted line at the top shows the $d_\perp$ of the fcc-Mn films grown on Cu_3Au(001) [11]. The crystalline structures of the c-fct Mn and e-fct Mn films, determined from the LEED and LEED I/V analysis, are shown at the top.

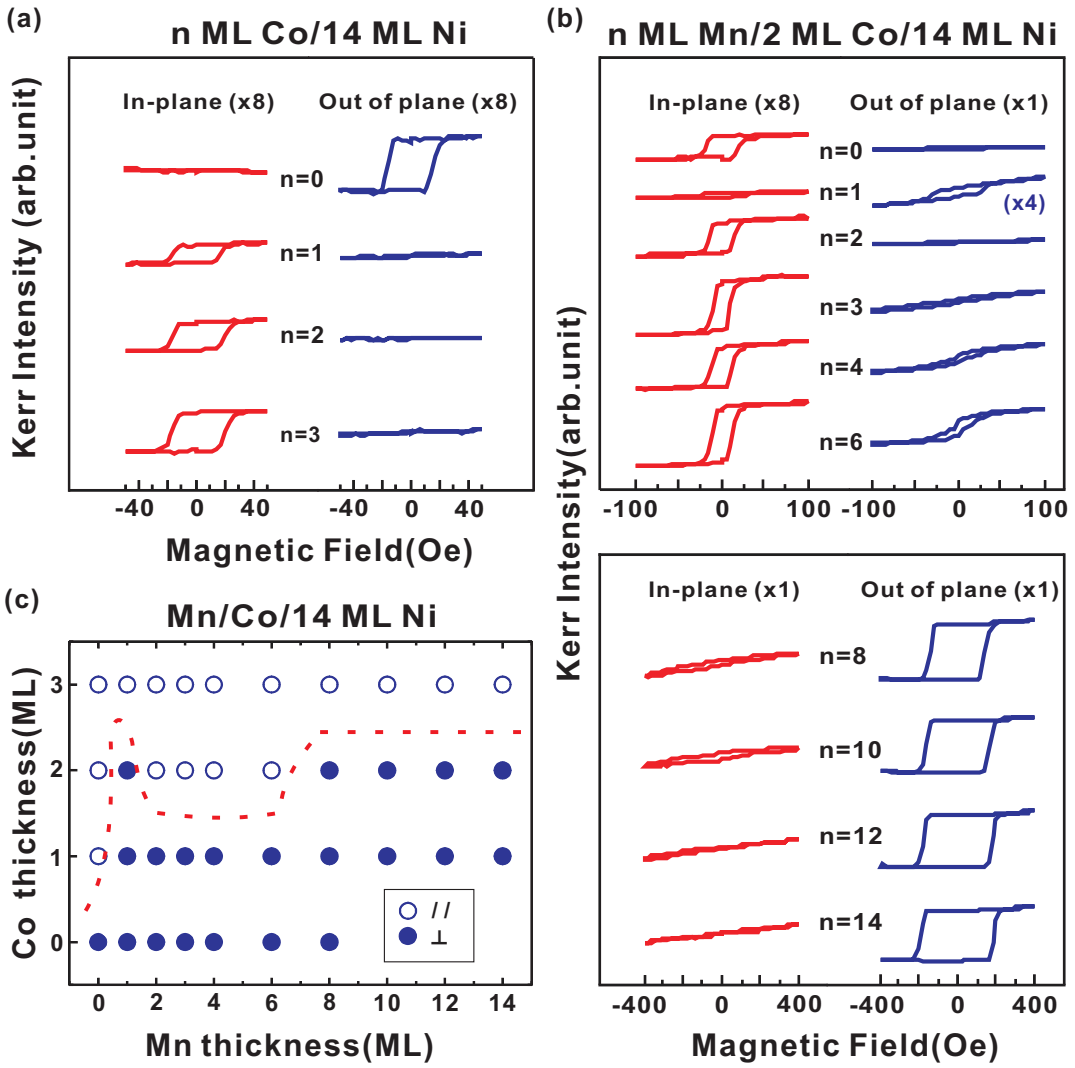

FIG. 4. (Color online) Magnetic hysteresis loops of (a) 0–3 ML Co/14 ML Ni/Cu(001) and (b) 0–14 ML Mn/2 ML Co/14 ML Ni/Cu(001) films. (c) Magnetic easy axis phase diagram of 0–14 ML Mn/0–3 ML Co/14 ML Ni/Cu(001) films, measured according to longitudinal and polar MOKE at 300 K. In (c), the dashed line represents the boundary between in-plane and perpendicular magnetization derived from the MOKE measurements.

along only the perpendicular direction. As the 1 ML Co film was introduced, the Co/Ni films exhibited a weak IMA and consequently changed to a PMA when the Mn films were further deposited, indicating that Mn films can induce a PMA on Co/Ni bilayers. When the 2 ML Co film was introduced, the IMA of the FM layers was considerably enhanced. Notably, a weak perpendicular magnetization was observed when single-layered Mn films were deposited [Fig. (4b)]. However, the PMA disappeared rapidly as the t_{Mn} value increased to 2 ML, and it was observed again when the t_{Mn} value was greater than 6 ML. This nonlinear magnetic anisotropy variation was not observed for the Mn/3 ML Co/14 ML Ni films, probably because of the dominant IMA of the Co layers.

According to previous reports [11,12], Mn films may induce a PMA on adjacent FM films through an AFM-FM exchange coupling. To clarify the correlation between the substantial SRT of the Mn/2 ML Co/14 ML Ni films and the antiferromagnetism of the fct-like Mn films, we compared the H_c values of the magnetic films; we used H_c for this comparison because an enhanced H_c is typically accepted as a standard indicator of the establishment of an AFM-FM exchange coupling as well as AFM ordering in AFM/FM bilayers [3,5]. Figure 5(a) displays the remanent magnetization of hysteresis loops of various Mn/2 ML Co/14 ML Ni films previously analyzed [Fig. (4b)], indicating the existence of a PMA at $t_{\mathrm{Mn}} = 1$ ML as well as at $t_{\mathrm{Mn}} > 6$ ML. For comparison, Figs. 5(b) and 5(c) show the perpendicular and in-plane H_c of various Mn/1–3 ML Co/14 ML Ni films, respectively. Clearly, the H_c is significantly enhanced as t_{Mn} exceeds 6 ML, regardless of whether the samples exhibit in-plane or perpendicular magnetization. This indicates a threshold thickness of 6 ML for the established long-range AFM ordering of the Mn films grown on the Co/14 ML Ni films. Notably, this long-range AFM ordering threshold (at $t_{\mathrm{Mn}} = 6$ ML) is also close to the critical Mn film thickness associated with the onset of PMA in the Mn/2 ML Co/14 ML Ni films [Fig. (5a)]. These results suggest that the PMA observed when the t_{Mn} value exceeds 6 ML is possibly induced by the AFM Mn films through the AFM-FM exchange

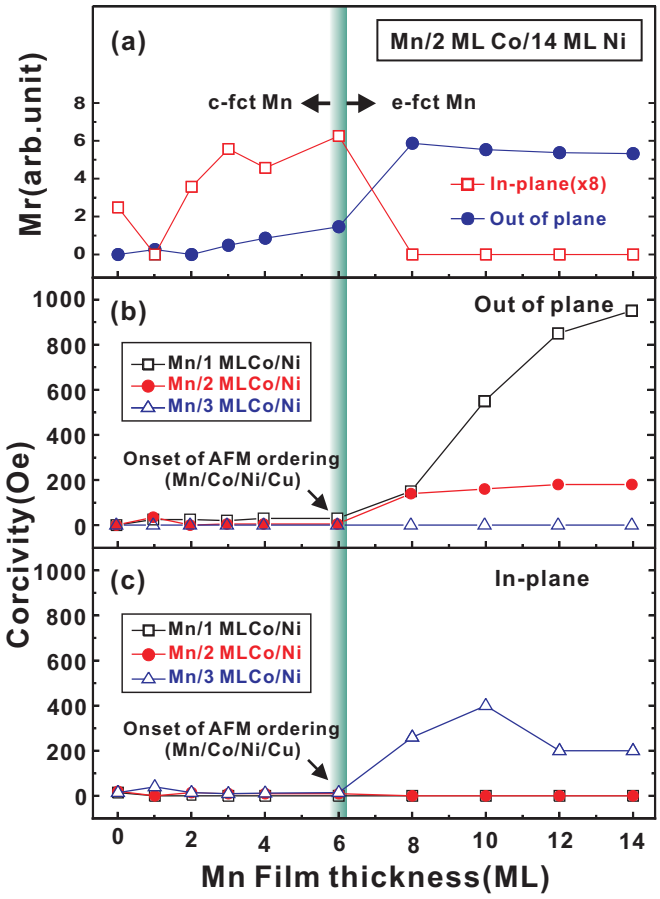

FIG. 5. (Color online) (a) Remanent magnetization (M_r) of the 0–14 ML Mn/2 ML Co/14 ML Ni/Cu(001) films measured at 300 K. (b) and (c) Out-of-plane and in-plane coercivity (H_c) of the 0–14 ML Mn/0–3 ML Co/14 ML Ni/Cu(001) films, respectively, measured at 300 K.

coupling, and this finding is consistent with those studies on FM/fcc-Mn [11] and CoO/Ni bilayers [13]. Notably, our LEED I/V analysis reveals that the critical SRT thickness (at $t_{Mn} = 6$ ML) occurred concurrently with the presence of e-fct Mn films [Fig. (3b)]. These findings suggest that the $d_\perp$ of the fct-like Mn films could be a critical factor influencing the occurrence of PMA in the Mn/2 ML Co/14 ML Ni films.

C. Observation of c-fct-Mn-film induced in-plane anisotropy through magnetic domain imaging

The preceding results clearly revealed that the e-fct Mn films (at $t_{Mn} > 6$ ML) induced PMA in adjacent Co/Ni films. However, the c-fct Mn films did not demonstrate PMA-inducing effects, and this might be caused by a lack of long-range AFM ordering at 300 K because of a lower coverage of film. To further clarify the PMA-inducing effects of the c-fct Mn films, temperature-dependent XMCD-PEEM measurements were performed. Direct magnetic domain imaging was applied to double wedge-shaped Mn/Co/14 ML Ni films (Figs. 6, top), because the magnetic anisotropy of films could be sensitive to variations in the thickness of both Mn and Co layers. In-plane ⟨110⟩ Ni magnetization directions were clearly observed for wedge-shaped 1–2 ML Co/14 ML Ni films at 300 K [Fig. (6a)]. When the Mn overlayer was deposited, the magnetization direction of the magnetic domain changed from in-plane to out-of-plane, reflecting an SRT of the Ni film in the Mn/Co/Ni layers. Figure 6(b) illustrates Ni domain images of wedge-shaped 2–5 ML Mn/1–2 ML Co/14 ML Ni films; in this figure, the structure of the Mn films is characterized as c-fct. Magnetic domains with perpendicular magnetization, as extended from the domains of Fig. 6(a), were observed in an area with a lower t_{Mn} value. The magnetization direction of the magnetic domain clearly changed from out-of-plane to in-plane when the t_{Mn} value was greater than a t_{Co}-dependent critical value, as indicated by the dashed line in this figure. In general, the area exhibiting perpendicular magnetization in Figs. 6(a) and 6(b) shrunk as t_{Co} increased because of the enhanced IMA induced by the thicker Co film. In this study, the magnetic anisotropy of the Mn/Co/Ni films derived from the magnetic domain imaging [Figs. 6(a) and 6(b)] is consistent with the measurements of the magnetic easy axis phase diagram [Fig. (4c)] on the basis of hysteresis loop measurements.

When the temperature decreased, the magnetization direction of the magnetic domains changed considerably. For wedge-shaped 0–0.7 ML Mn/1–2 ML Co/14 ML Ni films, the magnetic domains demonstrating PMA extended to areas with higher t_{Co} values when the temperature dropped from 300 [Fig. (6a)] to 105 K [Fig. (6c)]. Such a PMA enhancement was also observed in the left area of the domain images in Fig. 6(d) compared with Fig. 6(b) when t_{Mn} increased slightly. Because PMA enhancement was observed only for the FM films or Mn films with low layer coverage, the PMA phenomenon is attributed to a strengthened perpendicular crystalline anisotropy of the 14 ML Ni film or the ultrathin Mn films at low temperatures [12]. By contrast, in wedge-shaped 3–5 ML Mn/1–2 ML Co/14 ML Ni films [Figs. 6(b) and 6(d)], in which the structure of the Mn films was classified as c-fct, the magnetic domains exhibiting IMA expanded considerably to a region with a lower t_{Co} when the temperature was changed from 300 to 105 K. This IMA enhancement was possibly induced by the c-fct Mn films with a strengthened AFM ordering at low temperatures, rather than the Co/Ni films, because the results of Figs. 6(a) and 6(c) suggest that the Co/Ni films exhibit an enhanced PMA at low temperatures. Therefore, on the basis of the presented MOKE and temperature-dependent PEEM results, we can conclude that a PMA can be induced in FM films by ultrathin Mn films ($t_{Mn} < 2$ ML) or e-fct Mn ($t_{Mn} > 6$ ML) films. By contrast, c-fct Mn films with enhanced AFM ordering at low temperatures can induce IMA in the adjacent FM layers.

IV. DISCUSSION

A. Induced PMA through interfacial Mn moments

According to the results in Figs. 4(b) and 6(a), the 2 ML Co/14 ML Ni films exhibited PMA when covered with monolayered Mn films. Because the 1 ML Mn/Co/Ni/Cu(001) films showed only P(1 × 1) LEED spots similar to Cu(001) [Fig. (2c)], which indicated a minor effect of interdiffusion between this film and the Co film underneath, the induced PMA was not attributable to the alloying effect but to other effects. In

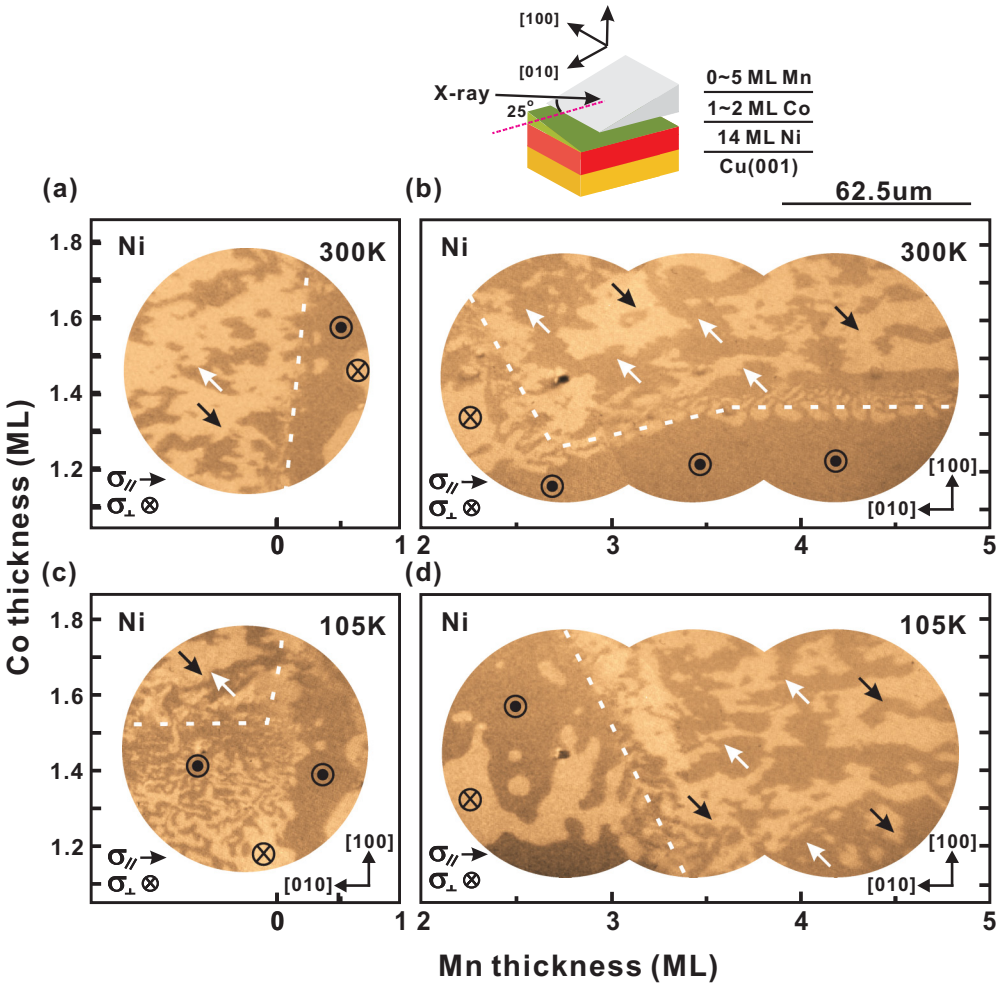

FIG. 6. (Color online) Ni domain images of the (a) wedge-shaped 0–0.7 ML Mn/1–2 ML Co/14 ML Ni/Cu(001) and (b) wedge-shaped 2–5 ML Mn/1–2 ML Co/14 ML Ni/Cu(001) films obtained with RCP x rays at 300 K. (c) and (d) Magnetic domain images of the wedge-shaped 0–1.5 ML Mn/1–2 ML Co/14 ML Ni/Cu(001) and wedge-shaped 2–5 ML Mn/1–2 ML Co/14 ML Ni/Cu(001) films measured at 105 K, respectively. In each figure, the $\sigma_{\parallel}$ and $\sigma_{\perp}$ at the bottom left denote the horizontal and vertical components of the photohelicity of the incident x ray with respect to the sample, respectively, as illustrated in the top cartoon. The magnetization directions of magnetic domains are indicated by the black/white or up/down arrows. The dashed line represents the boundary between in-plane and perpendicular magnetization. Notably, the Co magnetic domains are coupled in parallel with the Ni domains (as, for example, shown in Fig. 7). The spatial resolution of magnetic domains is estimated to be about 200 nm [36].

fact, PMA enhancement induced by uncompensated interfacial Mn moments was observed in Mn/Ni/Cu(001) [37], where the SRT (in-plane to out-of-plane) thickness of Ni/Cu(100) shifted to an area with thinner Ni after the Ni film was covered with 0.5 ML Mn [37,38]. Moreover, a considerably enhanced PMA was observed in Fe/fcc-Mn/Cu_3Au(001) [11] and was attributed to a coupling effect with uncompensated interfacial Mn moments with the establishment of a perpendicular crystalline anisotropy [12]. Similar to the findings of the aforementioned studies [11,12,37,38], we observed uncompensated magnetic moments for the Mn films [Fig. (7c)], which demonstrated an antiparallel coupling with the magnetic moments of the Co/Ni layers [Figs. 7(a) and 7(b)]. The corresponding x-ray absorption and XMCD asymmetry curves [Figs. 7(d) and 7(e)] were obtained by extracting the intensity of photoelectrons of individual Mn magnetic domains in Fig. 7(c) as a function of x-ray energy. In Fig. 7(e), the P and Q values are given by the integration of the XMCD asymmetry curve in L_3 and L_3-L_2 regions, which indicates the sum of magnetic asymmetry in both regions, respectively. In the XMCD sum rules [39–41], P and Q values can be used to calculate the ratio of orbital to spin moments according to the formula $m_{\text{orbital}}/m_{\text{spin}} = 2Q/(9P - 6Q)$ [41,42]. Thus, by applying the formula above, the out-of-plane $m_{\text{orbital}}/m_{\text{spin}}$ ratio of the uncompensated Mn moments of the 1 ML Mn/2 ML Co/14 ML Ni film is found to be 0.33. Such a value was sizable and close to that of the moments in Fe/fcc-Mn/Cu_3Au(001) [12].

According to previous reports [12,43], the strength of perpendicular crystalline anisotropy of magnetic films is linked to the out-of-plane $m_{\text{orbital}}/m_{\text{spin}}$ ratio. Thus, a finding of sizable out-of-plane $m_{\text{orbital}}/m_{\text{spin}}$ ratio for the uncompensated Mn moments in the 1 ML Mn/2 ML Co/14 ML Ni film suggests the establishment of a high perpendicular crystalline anisotropy of these moments. These uncompensated Mn

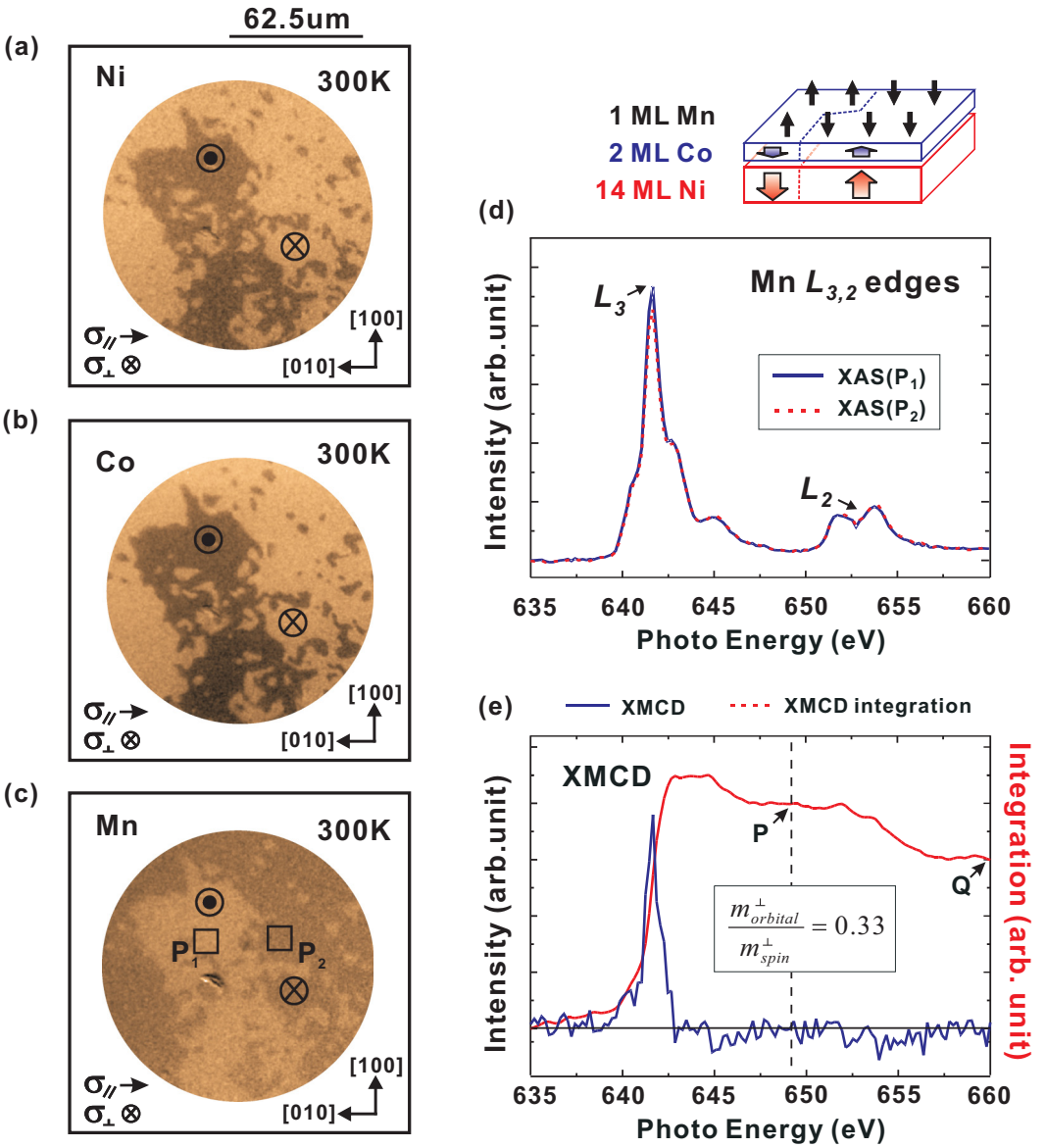

FIG. 7. (Color online) (a) Ni, (b) Co, and (c) Mn magnetic domain images of the uniform 1 ML Mn/2 ML Co/14 ML Ni/Cu(001) films measured at 300 K. The inverse magnetic contrast between Ni/Co and Mn domains indicate an antiparallel coupling between their magnetic moments. (d) Mn $L_{3,2}$ edge x-ray absorption (XAS) and (e) x-ray magnetic circular dichroism (XMCD) curves extracted from the P1 and P2 regions in (c). The spin/orbital ratio of Mn moments can be extracted from the integration of the XMCD curves according to the XMCD sum rules [41].

moments at FM/AFM interface are considered to be the origin of the PMA established in Mn/2 ML Co/14 ML Ni films. However, in contrast to the behavior of previously reported FM/fcc-Mn bilayers [11], in which the PMA magnitude was monotonically enhanced as t_{Mn} increased, according to the finite size tendency of low-dimensional antiferromagnets [20], the PMA of the Mn/2 ML Co/14 ML Ni films in the current study was considerably modulated when t_{Mn} was varied (Fig. 4). This difference may be induced by the invariant fcc structure of the Mn films in Fe/Mn/Cu_3Au(001) [Fig. (2b)] [11]; nevertheless, a c-fct to e-fct transition was observed in the Mn films in Mn/Co/14 ML Ni/Cu(001) at various t_{Mn} values. We thus suggest that the $d_\perp$ of fct-like Mn films is a crucial factor influencing the behavior of such films in inducing PMA in adjacent FM layers.

B. Correlation between the vertical interlayer distance of the Mn films and induced magnetic anisotropy in the fct-like Mn/Co/Ni films

A detailed discussion on the correlation between the $d_\perp$ of the fct-like Mn films and induced magnetic anisotropy on the Mn/Co/Ni films is imperative. As mentioned, uncompensated interfacial Mn moments may lead to a perpendicular crystalline anisotropy, which consequently induces PMA in adjacent FM film. [12,37,38] However, when the c-fct Mn or e-fct Mn films are deposited, the induced PMA may either be dissipated or enhanced. The different behaviors of the c-fct and e-fct Mn films in inducing magnetic anisotropy might be correlated with their dissimilar AFM spin structures. However, studies on spin-polarized scanning tunneling microscopy [10,44–46] have suggested in-plane layered AFM spin structures for the

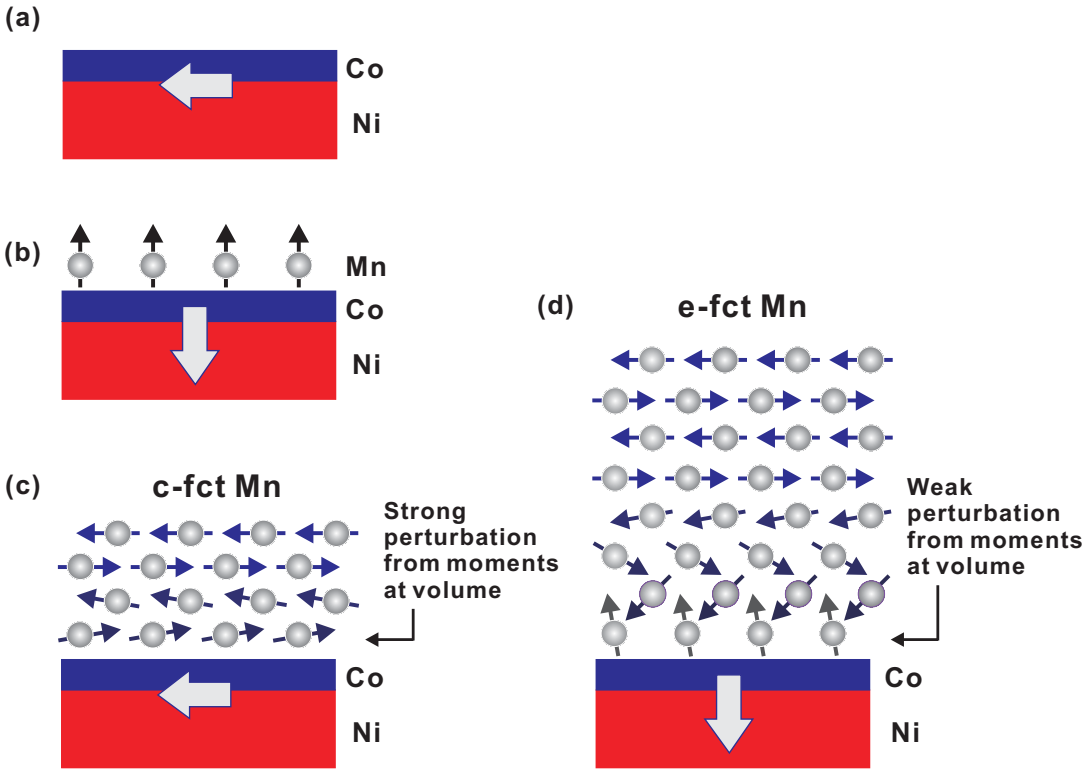

FIG. 8. (Color online) Schematic models of Mn/2 ML Co/14 ML Ni exchange-coupled systems with (a) no coverage of Mn films, (b) coverage of 1 ML Mn films, (c) coverage of c-fct Mn films, and (d) coverage of e-fct Mn films on Co/Ni films.

fct-like Mn films (either $c/a > 1$ or $c/a < 1$) grown on FM films. Therefore, the possibility that the different behaviors of inducing magnetic anisotropy caused by dissimilar AFM spin structures of two Mn films is considered to be minor. Instead, the $d_\perp$ of Mn films could be a highly crucial factor modulating the behaviors of such films in inducing magnetic anisotropy. A study suggested that contracting the atomic distance in fct-like Mn films could considerably enhance the strength of Mn-Mn exchange coupling [47]. According to this study, we speculate that varying $d_\perp$ in fct-like Mn films may also change the strength of the exchange coupling between interfacial Mn moments and moments within the volume, which perturbs the spin alignment of the Mn interfacial moments as well as the ability of inducing PMA in the present fcc-like Mn/Co/Ni/Cu(001) system.

For the c-fct Mn films with a lower $d_\perp$ value (approximately 1.71 Å), the exchange interaction between adjacent Mn layers is expected to be strong. As shown in Fig. 8(c), the spin alignment of interfacial Mn moments could be considerably affected by the coupling effects from the volume spins of Mn films with in-plane layered AFM ordering. In such a situation, the interfacial Mn spins may be forced to tilt in the in-plane direction, thus inducing IMA in the adjacent FM film, as indicated in temperature-dependent magnetic images of Figs. 6(b) and 6(d). By contrast, for the e-fct Mn films with a higher $d_\perp$ value (approximately 1.88 Å), the volume spins of the Mn films are expected to exert a lower perturbation effect on the interfacial Mn moments. The interfacial moments of the Mn films may remain in an out-of-plane orientation and still contribute to the PMA in the FM films, as demonstrated in a previous study [12]. The stability of the PMA of Mn moments at the interface may still be supported by the Mn moments at volume through the noncollinear type exchange interaction, as inferred from previous works [11,15,48] and illustrated in Fig. 8(d). Notably, comparing the systems exhibiting Mn-induced PMA revealed that the $d_\perp$ value of the Mn films was approximately 1.88 Å [11,15]. This value can possibly serve an optimal condition that can be applied to ensure that perpendicular interfacial Mn moments maintain a "magnetic interaction" with volume moments of Mn films. Although additional theoretical calculations might be necessary for adequately supporting the proposed physical concept, the present work provides solid evidence indicating that $d_\perp$ is a crucial factor responsible for the antiferromagnet-induced PMA in AFM/FM bilayers. In the future, it will be imperative to further investigate AFM-induced PMA in additional AFM/FM systems for application in perpendicular-based magnetic devices.

V. CONCLUSION

We systemically investigated the structural effects of AFM thin films on antiferromagnet-induced PMA in epitaxially grown fct-like Mn/Co/Ni/Cu(001) films. We demonstrate that antiferromagnet-induced PMA is highly sensitive to the interfacial moments of the AFM films and the magnetic interaction of such moments with the volume moments; moreover, antiferromagnet-induced PMA is susceptible to the $d_\perp$ of the AFM films. The investigation results improve understanding of the phenomenon of AFM-induced PMA

in AFM/FM layers and can facilitate the development of the next-generation perpendicular-based spintronic devices that exploit the crystalline structures of ultrathin AFM layers.

ACKNOWLEDGMENT

This work was partly supported by the Ministry of Science and Technology, Taiwan (Grant No. MOST 102-2112-M-018-006-MY3).

[1] S. Mao, Z. Gao, H. Xi, P. Kolbo, M. Plumer, L. Wang, A. Goyal, I. Jin, J. Chen, C. Hou, R. M. White, and E. Murdock, IEEE Trans. Magn. **38**, 26 (2002).
[2] W. Zhang, Y. Chen, and C. Hiner, J. Appl. Phys. **97**, 10N702 (2005).
[3] J. Nogués and I. K. Schuller, J. Magn. Magn. Mater. **192**, 203 (1999).
[4] S. D. Bader, Rev. Mod. Phys. **78**, 1 (2006).
[5] J. Stöhr and H. C. Siegmann, *Magnetism: From fundamentals to Nanoscale Dynamics*, illustrated ed. (Springer, New York, 2006).
[6] H. Ohldag, A. Scholl, F. Nolting, S. Anders, F. U. Hillebrecht, and J. Stöhr, Phys. Rev. Lett. **86**, 2878 (2001).
[7] W. Kuch, F. Offi, L. I. Chelaru, M. Kotsugi, K. Fukumoto, and J. Kirschner, Phys. Rev. B **65**, 140408 (2002).
[8] C. Won, Y. Z. Wu, H. W. Zhao, A. Scholl, A. Doran, W. Kim, T. L. Owens, X. F. Jin, and Z. Q. Qiu, Phys. Rev. B **71**, 024406 (2005).
[9] Q. F. Zhan and K. M. Krishnan, Appl. Phys. Lett. **96**, 112506 (2010).
[10] B. Y. Wang, C. H. Chuang, S. S. Wong, J. J. Chiou, W. C. Lin, Y. L. Chan, D. H. Wei, and M. T. Lin, Phys. Rev. B **85**, 094412 (2012).
[11] B. Y. Wang, N. Y. Jih, W. C. Lin, C. H. Chuang, P. J. Hsu, C. W. Peng, Y. C. Yeh, Y. L. Chan, D. H. Wei, W. C. Chiang, and M. T. Lin, Phys. Rev. B **83**, 104417 (2011).
[12] B.-Y. Wang, J.-Y. Hong, K.-H. Ou Yang, Y.-L. Chan, D.-H. Wei, H.-J. Lin, and M.-T. Lin, Phys. Rev. Lett. **110**, 117203 (2013).
[13] P. Kuświk, P. L. Gastelois, M. M. Soares, H. C. N. Tolentino, M. De Santis, A. Y. Ramos, A. D. Lamirand, M. Przybylski, and J. Kirschner, Phys. Rev. B **91**, 134413 (2015).
[14] N. Y. Jih, B. Y. Wang, Y. L. Chan, D. H. Wei, and M. T. Lin, Appl. Phys. Express **5**, 063008 (2012).
[15] B. Y. Wang, C. C. Chiu, W. C. Lin, and M. T. Lin, Appl. Phys. Lett. **103**, 042407 (2013).
[16] S. Mangin, D. Ravelosona, J. A. Katine, M. J. Carey, B. D. Terris, and E. E. Fullerton, Nat. Mater. **5**, 210 (2006).
[17] Y. Shiroishi, K. Fukuda, I. Tagawa, H. Iwasaki, S. Takenoiri, H. Tanaka, H. Mutoh, and N. Yoshikawa, IEEE Trans. Magn. **45**, 3816 (2009).
[18] S. Ikeda, K. Miura, H. Yamamoto, K. Mizunuma, H. D. Gan, M. Endo, S. Kanai, J. Hayakawa, F. Matsukura, and H. Ohno, Nat. Mater. **9**, 721 (2010).
[19] D. C. Worledge, G. Hu, D. W. Abraham, J. Z. Sun, P. L. Trouilloud, J. Nowak, S. Brown, M. C. Gaidis, E. J. Ó Sullivan, and R. P. Robertazzi, Appl. Phys. Lett. **98**, 022501 (2011).
[20] T. Ambrose and C. L. Chien, Phys. Rev. Lett. **76**, 1743 (1996).
[21] J. T. Kohlhepp and W. J. M. de Jonge, Phys. Rev. Lett. **96**, 237201 (2006).
[22] J. T. Kohlhepp, H. Wieldraaijer, and W. J. M. de Jonge, Appl. Phys. Lett. **89**, 032507 (2006).
[23] J. T. Kohlhepp, J. Phys. D: Appl. Phys. **40**, 1300 (2007).
[24] M. T. Lin, W. C. Lin, C. C. Kuo, and C. L. Chiu, Phys. Rev. B **62**, 14268 (2000).
[25] J. Shen, J. Giergiel, and J. Kirschner, Phys. Rev. B **52**, 8454 (1995).
[26] W. C. Lin, C. C. Kuo, C. L. Chiu, and M. T. Lin, Surf. Sci. **478**, 9 (2001).
[27] J. Stöhr, Y. Wu, B. D. Hermsmeier, M. G. Samant, G. R. Harp, S. Koranda, D. Dunham, and B. P. Tonner, Science **259**, 658 (1993).
[28] C. M. Schneider and G. Schönhense, Rep. Prog. Phys. **65**, R1785 (2002).
[29] M. Zheng, J. Shen, P. Ohresser, Ch. V. Mohan, M. Klaua, J. Barthel, and J. Kirschner, J. Appl. Phys. **85**, 5060 (1999).
[30] W. Platow, U. Bovensiepen, P. Poulopoulos, M. Farle, K. Baberschke, L. Hammer, S. Walter, S. Müller, and K. Heinz, Phys. Rev. B **59**, 12641 (1999).
[31] C. H. Wang, Y. Y. Huang, and W. C. Lin, J. Appl. Phys. **109**, 103908 (2011).
[32] B. Schirmer, B. Feldmann, A. Sokoll, Y. Gauthier, and M. Wuttig, Phys. Rev. B **60**, 5895 (1999).
[33] W. C. Lin, T. Y. Chen, L. C. Lin, B. Y. Wang, Y. W. Liao, K. J. Song, and M. T. Lin, Phys. Rev. B **75**, 054419 (2007).
[34] J. Hafner and D. Spišák, Phys. Rev. B **72**, 144420 (2005).
[35] T. Burkert, O. Eriksson, P. James, S. I. Simak, B. Johansson, and L. Nordström, Phys. Rev. B **69**, 104426 (2004).
[36] D.-H. Wei, Y.-L. Chan, and Y.-J. Hsu, J. Electron Spectrosc. Relat. Phenom. **185**, 429 (2012).
[37] C. S. Tian, Z. Tian, J. Wu, G. S. Dong, X. F. Jin, Y. Z. Wu, and Z. Q. Qiu, J. Magn. Magn. Mater. **286**, 497 (2005).
[38] D. Schmitz, O. Rader, C. Carbone, and W. Eberhardt, Phys. Rev. B **54**, 15352 (1996).
[39] B. T. Thole, P. Carra, F. Sette, and G. van der Laan, Phys. Rev. Lett. **68**, 1943 (1992).
[40] P. Carra, B. T. Thole, M. Altarelli, and X. Wang, Phys. Rev. Lett. **70**, 694 (1993).
[41] C. T. Chen, Y. U. Idzerda, H. J. Lin, N. V. Smith, G. Meigs, E. Chaban, G. H. Ho, E. Pellegrin, and F. Sette, Phys. Rev. Lett. **75**, 152 (1995).
[42] The magnetic dipole operator term has been negligible, because it is small for 3*d* metals [49].
[43] P. Bruno, Phys. Rev. B **39**, 865 (1989).
[44] U. Schlickum, N. Janke-Gilman, W. Wulfhekel, and J. Kirschner, Phys. Rev. Lett. **92**, 107203 (2004).
[45] P.-J. Hsu, C.-I. Lu, Y.-H. Chu, B.-Y. Wang, C.-B. Wu, L.-J. Chen, S.-S. Wong, and M.-T. Lin, Phys. Rev. B **85**, 174434 (2012).
[46] T. K. Yamada, M. M. J. Bischoff, G. M. M. Heijnen, T. Mizoguchi, and H. van Kempen, Phys. Rev. Lett. **90**, 056803 (2003).

[47] B.-Y. Wang, J.-Y. Hong, N.-Y. Jih, K.-H. Ou Yang, L.-R. Chen, H.-J. Lin, Y.-L. Chan, D.-H. Wei, and M.-T. Lin, Phys. Rev. B **90**, 224424 (2014).

[48] Y. Y. Wang, C. Song, G. Y. Wang, F. Zeng, and F. Pan, New J. Phys. **16**, 123032 (2014).

[49] R. Wu, D. Wang, and A. J. Freeman, Phys. Rev. Lett. **71**, 3581 (1993).